Observation of the Mouse Tissues in Open Aqueous Solution by Atmospheric Scanning Electron Microscope

Nassirhadjy Memtily

Graduate School of Comprehensive Human Sciences,

University of Tsukuba

Abstract

The structure-function relationships in tissues are key to understand their mechanisms, which should be precisely studied using microscopy. Standard electron microscopy (EM) has subnanometer or nanometer resolution, but samples must be observed in vacuum. For biological samples, a transmission electron microscopy (TEM) observation requires time consuming tissue preparation including fixation, dehydration, embedding, ultra-thin sectioning and staining. In the case of a scanning electron microscopy (SEM) observation, the specimens have to be fixed, dehydrated and coated with metals or carbon. On the other hand, in the atmospheric scanning electron microscope (ASEM), a 2 – 3 μm-thick layer of the sample can be observed at atmospheric pressure without dehydration. During the operation, handling of small specimen is possible because it is equipped with an open specimen holder and an optical microscope (OM) above the specimen.

In this study, various mouse tissues, i.e., brain, muscle, heart, lung, liver, kidney, spleen and digestive tract (esophagus, small intestine and stomach) stained with heavy metals and placed in a solution containing radical scavenger D-glucose solution were observed by ASEM for the first time. While the staining regents such as platinum-blue and phosphotungstic acid made the nuclei of cells very prominent, others, such as uranium acetate or the NCMIR method stained intracellular organelles and membranous structures. In cerebrum and cerebellum, layer structures of nerve cells in solution were clearly imaged and fine intra- and inter- layer connections were visualized. In myocytes of cardiac and skeletal muscles, sarcomere striations was clearly visualized. Typical regular longitudinal smooth myocytes surrounded by a network of neurons were

observed in small intestine. Interestingly, mucosa of the stomach lumen were observed together with symbiotic bacteria. In the kidney tissue, Bowman's capsules, glomeruli, proximal or distal convoluted tubules and podocytes were successfully imaged. Spleen was observed to have many different shaped blood cells, including lymphocytes. These results suggest that ASEM has enough resolution for observation of normal tissues without time consuming tissue preparation processes. Furthermore, kidney tissue could be stained and successfully imaged within just 30 minutes. Lung and spinal cord tissue from mice metastasized with breast cancer cells and its control were also examined. Cancer cells were found to be present in alveoli and in parts of the spinal cord having clearly larger nuclei than normal cells.

In conclution, the results indicate that the ASEM can be applied for the intra-operative cancer diagnosis, the diagnosis of kidney diseases and the pathogen detection. Increase in the observable tissue area by using a new multi-windowed ASEM sample dish, and sliding the tissue across its 8 windows are considered to increase the possibility to apply ASEM to a clinical diagnosis.

Abbreviations

A band, anisotropic band;

ASEM, atmospheric SEM;

CL, cathodoluminescence;

EM, electron microscope/microscopy;

EP, motor end-plate;

GA, glutaraldehyde;

I band, isotropic band;

ID, intercalated disk;

LC, lead citrate;

NCMIR, National Center for Microscopy and Imaging Research;

OM, optical microscope/microscopy;

PB, phosphate buffer;

PBS, Phosphate buffered saline;

PFA, paraformaldehyde;

PTA, phosphotungstic acid;

SEM, scanning electron microscope/microscopy;

SiN, silicon nitride;

TEM, transmission electron microscope/microscopy;

TI-Blue, Platinum Blue, $Pt_4(NH_3)_8(C_6H_{13}O_5)_4$;

THC, tetrahydrocannabinol;

UA, uranyl acetate.

1. Introduction

The precise understanding of the structure of tissues is key to understand the mechanisms of their function, which have been studied utilizing various microscopies. Optical microscopy (OM) has been developed in various ways and has led to great discoveries and advances in biology and medicine (Golgi C, 1898; Hell SW, 2007). The microscopic spesimens of tissue samples are either prepared by time-consuming paraffin embedding and sectioning, or quick freezing followed by cryo-sectioning. Paraffin-embedding is widely used in basic biological studies, applied biology fields and medicine. On the other hand the tissue biopsies are often cryo-sectioned, stained by hematoxylin-eosin (HE) and inspected during surgery performed to remove tissues suffering from cancer invasion and metastasis (Ferreiro JA, et al., 1995; Wilson LB, 1905). However, cryo-thin-sectioning is quite difficult and takes about 15-30 minutes for each sample (Sato C, 2011b). Thus, cryo-thin-sectioning can prolong the whole operation, which is a burden for patients. Moreover, freezing might slightly affect nuclei morphology (Bauermeister DE, 1980;Riedl O, et al., 2009;Wada N, et al., 2004). The size of cell nuclei is the most significant indicator used for the intraoperative cancer diagnosis; the nucleus of cancer cells is usually larger than that of normal cells.

Standard transmission electron microscopy (TEM) using resin thin-sectioning has subnanometer or nanometer resolution, but samples must be observed in vacuum. For biological samples, this basically means time-consuming pretreatment, including hydrophobic procedures. Thin-sectioning of samples directly embedded in hydrophilic resin is possible without dehydration, though it requires considerable technical skill. Also, the thin-sectioning can restrict information to within a thin slice, if

continuous-sectioning is not performed. The sample pretreatment required for conventional scanning electron microscopy (SEM) of biological samples generally includes fixation, heavy metal staining, dehydration, drying and metal coating, which precludes observation of internal structures.

Optical microscope can directly visualize wet structure, although even a super high-resolution microscopy which requires special fluorescence labeling has a resolution limit of around 50 nm. Consequently, there is a huge missing mesoscopic scale in microscopy. Observation of subcellular supercomplexes and organelles of cells is important for understanding tissue function.

Since the first Environmental cells were reported in 1944 (Abrams IM & McBain JW, 1944), in solution electron microscopy has been one of the most important topic for high-resolution imaging. With the improvement in new semiconductor fabrication technologies, tough, almost electron-transparent films have greatly improved Environmental cells (de Jonge N, et al., 2009; Williamson MJ, et al., 2003). Stronger membrane windows have been developed, facilitating the development of different types of Environmental cells with small electrodes or microfluidic systems (Ring EA & de Jonge N, 2010; Williamson MJ, et al., 2003). Environmental cells have achieved significant breakthroughs in the field of ligand- and antibody-labeled EM, visualizing samples in solution without artifacts due to the dehydration process. The surface level of tissue blocks excised from various organs has been successfully observed in an environmental capsule by scanning electron microscopy (SEM): heart and kidney (Thiberge S, et al., 2004), kidney (Nyska A, et al., 2004), brain tumor (Bahar V, 2005; Barshack I, et al., 2004b) liver, sciatic nerve, spinal cord (Kristt D & Nyska A, 2007), colon (Barshack I, et al., 2004a). However, there are few shortcomings in this device.

Although some environmental cells are semi-closed with inlet- and outlet-tubes, the capsule configuration generally tends to preclude the administration of reagents during the experiment. The capsules are also very small, holding only up to 15 µl of liquid. This size and volume restrict the cell species that can be cultured within them. The limited volume also makes it hard to observe phenomena accompanying volume change, e.g., involving gas generation and liquid evaporation.

These capsules allows 'wet' samples to be examined in the vacuum of the microscope, avoiding dehydration artifacts. However, the environmental capsule for the SEM has a capacity of only about 15 µl, the samples are not accessible, e.g., for additional staining or manipulation (Nishiyama H, et al., 2010).

Another trend is the development of correlative microscopy, which combines various EM systems with OM. Many microscopes based on TEM and SEM were developed (Agronskaia AV, et al., 2008; Sartori A, et al., 2007). However, simultaneous direct link between OM and EM was not easy using these machines.

The Atmospheric SEM (ASEM) ClairScope™ has an inverted SEM configuration, and was developed to realize SEM observation of a sample at atmospheric pressure in a readily-accessible, open container (ASEM dish) (Nishiyama H, et al., 2010). An OM positioned above the dish can be used to observe wide areas of the sample, and the smaller regions can be observed by the SEM through a thin silicon nitride (SiN) film in the base of the ASEM dish, in a fully correlative manner with OM. From below the ASEM dish, the inverted SEM emits an electron beam up through the SiN film, and beam scan the sample. Backscattered electrons are detected for imaging by the flat disk-shaped Backscattered Electron Imaging (BEI) detector which is located just beneath the SiN film, encircling the electron beam. As part of the whole imaging

process, an optical microscope (BXFM system, Olympus Co.) views the sample quasi-concurrently from above (Fig.1A). The optical axes of both microscopes are aligned and fixed to ensure that correlative images are recorded, and the specimen stage can move two-dimensionally (x-y) for targeting. The ASEM system, including the software, is named ClairScope. Consequently, ASEM realized simultaneous correlative microscopy. During the operation, handling of small specimen is easy because OM located above the sample can monitor the manipulation. The observable specimen depth of ASEM was 2-3 μm at 30 kV (Maruyama Y, et al., 2012b; Suga M, et al., 2009), and the resolution was 8 nm near the SiN membrane, which is advantageous for the observation of intercellular connections and fine subcellular structures. The SiN-windowed ASEM dish is a standard plastic Petri dish 35 mm in diameter, with a maximum capacity of almost 10 ml. The detachable open ASEM dish brought two other advantages: a large variety of cell types including neurons are easily culturable, and labeling-washing-staining cycles are quick and efficient (Hirano K, et al., 2014; KinoshitaT, et al., 2014; Maruyama Y, et al., 2012a; Nishiyama, et al., 2011; Sato C, 2011a). Culture conditions are stable, due to the large volume of the open dish and to the large surface area of the culture medium, which facilitates gas exchange in a CO_2 incubator. It has been reported that the primary cells from various mammalian (Hirano K, et al., 2014; Maruyama Y, et al., 2012b) and insect organs (Hirano K, et al., 2014; KinoshitaT, et al., 2014), including mouse hippocampus, cortex and cerebellum, and from prokaryotes, including coccus, bacillus (Hirano K, et al., 2014; KinoshitaT, et al., 2014; Maruyama Y, et al., 2012b) and mycoplasma (Sato C, et al., 2012) were successfully cultured. The cultured cells were fixed, stained with different heavy metal solutions, and imaged (Nishiyama H, et al., 2010). Because the epitopes of cultured

cells were preserved in aqueous solution, it was possible to successfully immunolabel different cells with various antibodies (Akita M, et al., 2013; Maruyama Y, et al., 2012a; Maruyama Y, et al., 2012b; Murai T, et al., 2013; Nishiyama H, et al., 2014). It has been outlined briefly that TI-Blue-stained brain of a gold fish was successfully observed by ASEM (Nishiyama H, et al., 2010).

Here I report the observation of various mouse tissues by ASEM after staining with various heavy metals and indicate the possibility of application of ASEM in the diagnosis of cancer and kidney diseases. Staining with PTA or TI-Blue made cell nuclei very prominent, while staining with UA or modified NCMIR method clearly revealed cell outlines and organelles together with extracellular structures. The difference between cancer-metastasized lung and its control were successfully visualized. Importantly, the observable area was enlarged by the use of a new multi-windowed ASEM dish and by exploiting the open ASEM dish configuration to slide tissue across the windows.

2. Purpose of this study

Since optical microscopies of tissues basically require time-consuming thin-sectioning, I aim to develop a SEM method to observe a thin-surface layer of a specimen immersed in natural aqueous solution by exploiting the penetrating depth of an electron beam and its backscattering electrons. For this goal, the ASEM system can be employed, the vacuum of the inverted SEM column being separated from the sample holder using electron permeable SiN film of the ASEM dish. Because the electron beam diameter of SEM is smaller than 10 nm, a high resolution can be expected. The small contrast of biomaterials is expected to be enhanced by developing heavy metal staining methods, realizing differential staining of various cell components to facilitate studies of structure-function relationships in various animals, plants and microbes. To increase observation efficiency, a tissue sliding method on the flat multi-windowed ASEM dish will be developed.

Since quick observation of tissue without thin-sectioning is also anticipated for intraoperative cancer diagnosis, application of the developed method to a mouse model of cancer metastasis will be attempted. If the developed method has high resolution, the applicability of this method to the study of host-microbe commensalism and to the diagnosis of kidney diseases should be studied, especially aiming at the diagnosis of primary glomerulopathies, which presently requires time-consuming Epon thin-section transmission EM.

3. Materials and methods

3.1 Animals

Six to fifteen week-old male and female ICR mice and 8 to 12 week-old female BALB/c mice (Japan Clea, Tokyo, Japan) were sacrificed to obtain normal and control tissue for observation. Tumor bearing mice were sacrificed 10 days after the intravenous injection of 4T1E/M3 breast cancer cells (1×10^6/mouse) or 30 days after the subcutaneous injection of the cells (1×10^6/mouse) to 8 week-old female BALB/c mice (Sakai H, et al., 2012; Takahashi M, et al., 2008; Takahashi M, et al., 2009). All experiments were approved by the Animal Care and Use Committee of the National Institute of Advanced Industrial Science and Technology (AIST), and were performed in accordance with the AIST Guidelines for Care and Use of Animals.

3.2 Tissue preparation

Animals were anesthetized using isoflurane (Abbott, Maidenhead, UK) and perfused with PBS from left ventricle followed by perfusion with 4% paraformaldehyde (PFA; Wako, Osaka, Japan) in phosphate buffered saline (PBS, 0.9% NaCl, in 0.05 M KH_2PO_4 / Na_2HPO_4 buffer, pH 7.4) (Kurokawa M, 2005). Tissues were either cut with a scalpel to obtain 1-2 mm thick tissue slabs or sliced with a PRO7 linear slicer (Dosaka, Kyoto, Japan) to obtain 100-200 μm thick slabs. Samples were washed several times with PBS, and further fixed with 4% PFA or 1% glutaraldehyde (GA) or with a solution containing the both fixatives for 30 minutes at room temperature. Spinal cord, esophagus, stomach and small intestine were cut into thick slab using scalpel after fixation, and stained.

3.3 Tissue preparation for OM.

Brain, lung, kidney, liver and spleen were harvested either from control and tumor bearing mice under the deep anesthesia by isoflurane. They were fixed in 10% neutral buffered formalin (Wako) at room temperature (RT) for 17-18 hours, dehydrated, embedded in paraffin. The tissues were cut into 5-6 μm sections, stained with HE, and examined under OM.

3.4 Heavy metal staining

Phosphotungstic acid (PTA) staining:

The fixed tissues were immersed in 0.5% Triton X-100 in PBS at room temperature for 15 minutes, and washed twice with PBS. Tissues were re-fixed in 1% glutaraldehyde (GA) in PBS, for 15 minutes. After washed twice with PBS, they were stained with 2% PTA in DDW for 3 hours at room temperature or overnight at 4℃.

Platinium-Blue staining:

The fixed tissues were treated in 0.5% Triton X-100 in PBS at RT for 15 minutes, and washed twice with PBS. They were stained with 0.6% platinum-blue (TI-Blue, Nisshin EM, Japan, 6% solution; $Pt_4(NH_3)_8(C_6H_{13}O_5)_4$) in PBS for 3 hours at RT or overnight at 4℃.

UA staining:

The fixed tissues were immersed in 0.5% Triton X-100 in PBS at room temperature for 15 minutes, and washed twice with PBS. Then these tissues were incubated with filtered 1% tannic acid, containing 1% GA for 30 minutes, and washed with DDW twice. They were stained with filtered 2 % uranyl acetate (UA) for 30 minutes.

Quick UA staining method:

Without prior treatment with Triton X-100, tissues were incubated with 2 % UA for 15 minutes at room temperature.

NCMIR staining method:

Tissues were stained using a slight modification of the NCMIR method by Ellisman's group (Deerinck TJ, et al., 2010). The fixed tissues were perforated with 0.5% Triton X-100 in PBS at RT for 15 min, washed with DDW, and further fixed with 2.5% GA, 2% PFA, in filtered 0.1 M phosphate buffer (PB, pH 7.4) containing 2 mM $CaCl_2$ at RT for 15 min. They were then washed using filtered 0.15 M PB containing 2 mM $CaCl_2$, and further fixed/stained with the same buffer supplemented with 1.5% potassium ferricyanide (Sigma-Aldrich, St. Louis, MO, USA), 2% aqueous osmium tetroxide (OsO_4) (Nisshin EM) solution at RT for 60 min. After washing with DDW, tissues were then incubated with filtered 1% thiocarbohydrazide (TCH; Tokyo Chemical Industry, Co., Ltd., Tokyo, Japan) at RT for 20 min, rinsed with DDW, further stained with 2% aqueous OsO_4 at RT for 30 min, rinsed with DDW, stained with 2% UA in DDW and kept at 4˚C overnight. Finally, after rinsing with DDW, the tissue samples were stained with 0.4% lead citrate (TAAB Laboratories Equipment) at RT for 2 min. Once fully stained, all samples were placed 'cut' face down in the ASEM dish immersed in radical scavenger solution and imaged as soon as possible by OM and SEM, as the contrast of the stains fades on storage.

After staining, all samples were placed in the ASEM dish with radical scavenger solution (10 mg/ml dextrose in DDW) and observed by ASEM.

3.5 Imaging

The ClairScope ASEM system (JASM-6200, JEOL Ltd.) was used to record EM images (Nishiyama H, et al., 2010). The standard 35 mm bio-ASEM dish was used; the 100-nm thick, (250 × 250)-μm SiN film window built into its base separates the sample immersed in solution from the vacuum inside the SEM column. Alternatively, a newly-developed dish, with eight 100-nm thick, (250 × 250)-μm SiN film windows was employed to observe larger areas. After fixation and staining, tissues were placed on the SiN film window, and covered with 10 mg/ml (w/v) dextrose in DDW, and examined by ASEM. When the uneven surface of tissue prevented it from attaching well to the film, 150-250 Pascal pressure was applied during imaging. To guarantee the attachment of slab to the SiN film, a cover glass was placed on top of the tissue and loaded with a lead weight. The acceleration voltage of the SEM was 30 kV, and electrons backscattered from the cells were recorded for visualization. Since heavy metals scatter electrons, more heavily stained regions are observed bright in the SEM images.

3.6 Sliding a stained tissue slab across the ASEM dish.

A stained tissue slab was placed on the ASEM dish windows as described, and imaged by the inverted SEM from underneath. The tissue was then pushed slightly to the side with tweezers under monitoring by OM from above. The tissue was again imaged by SEM, and the images before and after the horizontal movement were merged.

4. Results

In this study, ASEM was found to be able to image a variety of mouse tissues. In each case, tissue slabs were stained with heavy metal solution, placed on the SiN film of the ASEM dish cut face down, and observed in aqueous solution using ASEM.

4.1 Neural tissues

Neural tissues from mice fixed by perfusion of 4% PFA in PBS were dissected into 1 - 2 mm thick slabs. After the treatment with Triton X-100, each tissue slab was stained with PTA, and imaged by ASEM. In cerebrum, observation of the surface level of the tissues revealed that neurons extend their neurites to form fine networks (Fig. 2A-C). In the cerebellum, three distinct cortical layers were observed; they are molecular layer, Purkinji cell layer, the granular layer as well as cerebellar white matter (Fig. 3D). Again, neurons were connected by delicate systematic networks (Fig. 2E and F). At the higher magnification, nuclei including brightly stained patches, presumably hetero chromatin and nucleoli were observed (Fig. 2F). These results are consistent with those obtained by HE staining and OM (Fig. 2A and Fig. 3A).

4.2 Cardiac muscle

In the cardiomyocytes, the heavily stained nuclei were observed as blurred white ellipsoid structure, the blurring probably being attributable to their distant location from the supporting SiN film (Fig. 4C and D). Between cardiomyocytes, an intercalated disc (ID) was clearly observed. Dark bands and bright bands were imaged by ASEM. The

alternating dark and bright bands imaged by ASEM can be interpreted as thin dark zones (I-bands) and broad bright zones (A-bands) of myofibril sarcomers.

4.3 Skeletal muscle

Muscle fibers were clearly visible when PTA-stained tissue slabs of gastrocnemius muscle were observed by ASEM (Fig. 5). The myocytes were found to be surrounded by filaments (Fig. 5A-B). In myocytes, I-bands, and A-bands were visualized as dark zones and broader bright zones, respectively, and Z-lines were frequently distinguished as a fine thin line in the center of dark I-bands (Fig. 5C). These results suggest that myocytes can be easily imaged at high resolution using the ASEM.

4.4 Digestive tract and attached nerves

Organs of the alimentary canal were observed by ASEM to further examine the applicability of the method. Esophagus, stomach and small intestine tissues were stained with PTA and imaged, unless otherwise specified (Fig. 6). The musculus externa of the pars cervicalis of esophagus looked very similar to gastrocnemius muscle (compare Fig. 6A with Figs 5). At higher magnification, longitudinal muscle fibers were observed to have dark zones corresponding to I-bands, broad bright zones corresponding to A-bands, and an attached network (Fig. 6B). After fixation, stomach was cut into pieces, stained with PTA then placed on an ASEM dish mucosal surface down and observed by ASEM for detecting symbiotic bacteria. Mucosa of the stomach lumen were observed together with symbiotic bacteria (Fig. 6C-D); a bacteria colony can be seen in Fig. 6D. Staining with the modified NCMIR method revealed the presence of another spcies of the symbiotic bacteria of different size (Fig. 6E-F). In the musculus externa of the small

intestine, elongated smooth muscle cells were observed after staining with PTA (Fig. 6G). A faint bright network of filaments runs on their surface, and is presumably formed by neurons (Fig. 6H). The nuclei of myocytes were visible together with erythrocytes.

4.5 Liver

When liver tissue slabs were stained with PTA, hepatocytes, sinusoids and central vein in the surface layers were clearly visualized by ASEM (Fig. 7 B-D). Nuclei of hepatocytes and nucleoli were also distinguished (Fig. 7 C-D). The overview is consistent with that of OM images obtained from HE stained paraffin embedded section (Fig. 7A).

4.6 Kidney

A slab excised from a mouse kidney was imaged by ASEM after fixation, permeation and staining with PTA (Fig. 8). In the cortex, Bowman's capsules, glomeruli, proximal or distal convoluted tubules and also podocytes–like cells were visualized (Fig. 8B). The overview is consistent with OM images obtained from HE stained paraffin embedded section.

4.7 Spleen

HE-stained thin-slices of spleen were observed by OM, revealing a large number of lymphocytes in the white pulp (Fig. 9 A). At higher magnification using ASEM, nuclei have brightly stained patches, presumably nucleoli and chromatin (Fig. 9F compare Fig. 3F and 7D). Reticular fiber-like fibrous structures less than 2 μm in thickness, were also

observed. These results are consistent with those obtained by HE staining and OM (Fig. 9A).

4.8 Observation of the lung metastasized by breast cancer and its control

The lung is known to be an organ easily metastasized by cancer. Lung tissues excised from control mice and from mice with tumors induced by the injection of breast cancer cells, were stained with both TI-Blue and PTA and observed by ASEM. For comparison, OM of HE-stained thin lung sections from other control and metastasized mice were shown in Fig.10A and 10E. In the control lung tissue, typical thin-wall structures with alveoli, alveolar ducts, a venous system were observed by ASEM (Fig. 10B-D). In the cells located at the surface of the tissue slab, nuclei were observed brightly. Their outlines were clear, enabling the measurement of their diameter. By contrast, only faint traces of the regular alveoli and alveolar ducts were discernible in metastasized lung (Fig. 10F-H). Most of the alveolar tissue was occupied by clusters of breast cancer cells, which have larger nuclei than those of lung epithelial and stromal cell (Fig. 10H). These results are consistent with those obtained by HE staining and OM (Fig. 10A and E), suggesting that ASEM can be applied to cancer diagnosis.

4.9 Observation of the spinal cord metastasized by breast cancer and its control

Slabs of spinal cord excised from the mice with tumors induced by the injection of breast cancer cells were stained with both TI-Blue and PTA without prior sectioning, and observed in comparison with those from the control mice using the ASEM. Isolated cells with larger nuclei were detected which were similar in size to those seen in lung metastasized with breast cancer cells (Fig. 11).

4.10 Quick observation of the lung metastasized by breast cancer.

Control lung and the lung metastasized by breast cancer cells were fixed, quickly stained with UA for just 15 min without Triton X-100 treatment, and observed by ASEM. The results (Fig 12A-F) were comparable with those shown in which the tissue slabs were treated with Triton X-100 and stained with TI-Blue and PTA (Fig. 10). The nuclei located closely to the surface of tissue slabs were clearly observed, and the size difference between normal and cancer cells were clear. These results suggest the potential of the quick method for intraoperative cancer diagnosis.

4.11 Wide area observation by sliding tissue on the ASEM dish.

To enlarge the area observable by ASEM, a spinal cord slab stained with PTA was placed in a newly developed 8-window ASEM dish and the tissue was repeatedly induced to slide very slightly across the thin membrane windows and imaged (Fig. 13A). Although the observable area in each ASEM imaging step was restricted to the field of the 8 windows, two sequential images partly overlapped and could be merged, covering a wider area of the spinal cord (Fig. 13C-F). The observable area of the multi-windowed dish (Fig. 13B) was thus successfully extended. The shift of the tissue on flat bottom surface of the ASEM dish (Fig. 13A) was precisely monitored by OM from above. This was made possible by the open ASEM dish configuration and the axis-aligned OM (Fig. 1A). In the future, the procedure could be automated by constructing a micro motor-driven manipulator to realize an accurate shift at regular time intervals, synchronized with ASEM scanning.

5. Discussion

SEM has proved to be very important for the study of morphology, especially of the surface structure of tissues. To prevent deformation artifacts, tissue samples generally require time-consuming pretreatment, including dehydration and metal coating, before they are placed in the vacuum of the microscope. Further, metal coat of tissues makes it impossible to observe the inside structure of the cells. In contrast, metal coating and the other tedious sample pretreatments are not required for ASEM. This unique imaging technique has many special characteristics. First, samples can be observed in aqueous solution at atmospheric pressure. This is made possible by the use of an open dish-shaped sample holder and an inverted SEM. The former seals the top of the SEM column and has a thin SiN-film window in its base, allowing SEM images of the sample to be obtained from below. Second, an OM positioned above the ASEM dish enables one to manipulate the sample during observation. Third, the electron conducting aqueous solution employed eliminates charging of the sample. Fourth, the detection of backscattered electrons allows observation of structures in a layer of 2-3 □m in thickness beneath the surface of the specimen resting on the flat SiN-film window when the SEM is operated at an accelerating voltage of 30 kV (Maruyama Y, et al., 2012b; Suga M, et al., 2009; Suga M, et al., 2011). These characteristics, taken as a whole, made it possible that diced and stained tissues can be viewed by ASEM quickly without further thin-sectioning, providing the information not only of the surface of the tissue but also the intracellular structures near the SiN film.

The oxidized surface of the SiN film, SiO_x, formed during the semiconductor making process is considered to have a glass-like nature. Certain cell types e.g., HEK, COS,

HELA and B16 melanoma cells, can grow directly on this film as well as on the glass base of the sample dish. The adhesion of primary cells from mouse tissues was facilitated if the surface of the film was coated by poly-L-lysine or proteins of extracellular matrix (Hirano K, et al., 2014; KinoshitaT, et al., 2014; Maruyama Y, et al., 2012a). As a hippocampus slice from mammalian brain has been successfully cultured on cover glass, organotypic cultures (Gähwiler BH, et al., 1997; Gahwiler BH, 1981) are highly expected to be grown on the ASEM dish and studied at high resolution. Because the dish accommodates 2 ml of liquid, it provides a stable culture environment for tissues or cells. The delicate handling of a small volume of liquid of a tiny piece of tissue, that are required for an environmental capsule are not required for ASEM. Furthermore, the ASEM with its open sample holder facilitates the administration of drugs (Nishiyama H, et al., 2014), making an application for drug screening possible. The open configuration of the ASEM dish also enables micro-injection or electrophysiology of tissues, under the monitoring by OM.

In this study, various staining reagents, including UA, TI-Blue, PTA, OsO_4 and lead citrate, were employed for tissue observation by ASEM. In particular, the bright images of chromatin and nucleoli observed in nuclei stained with TI-Blue and/or PTA (Figs. 3F, 7D and 9F) suggest that these reagents can be used to visualize chromatin in the nucleus. This, together with earlier images of chromosomes (Nishiyama H, et al., 2010), raises the possibility of applying TI-Blue/PTA staining and ASEM to chromatin related fields, e.g., spermatology. High resolution karyotyping using ASEM might help to find slight chromosomal deviations that are difficult to observe at present.

After a simple PTA staining, ASEM visualized a bacteria colony on the mucosal side of stomach tissue (Fig. 6C-D). If the time for the staining can be shortened, ASEM is considered to have a potential to detect bacteria in a tissue sample without application of bacteria culture, which would be especially important for infectious bacteria that are viable but non-culturable (VNC bacteria), or for anaerobes, that takes longer time (several days) to culture for diagnosis. ASEM can be further applied to visualize the infiltration of bacteria into tissue regions and the inflammation they trigger during surgery and treatment. The modified NCMIR staining method involving the use of OsO_4 (Deerinck TJ, et al., 2010) clearly visualized membranous structures at high contrast, not only for eukaryotic cells but also for prokaryotes (Fig. 6E and F). It could be used to study the symbiotic bacteria that are necessary to establish natural immunity, and also commensal bacteria, including *Helicobactor pylori*.

During intraoperative cancer diagnosis, the sizes of cell nuclei are usually determined by cryo-sectioning tissue excisions, staining them with HE and observing them by OM. However, this method using cryo-thin sectioning takes at least 15–30 minutes, leaving the tumor excision suspended. Among the processes involved in the diagnosis, cryo-thin sectioning is time consuming and the most difficult. Due to the difficulty of this step, diagnosis is sometimes confirmed later by paraffin-thin sectioning or sometimes by antibody labeling, involving the possibility of further surgery. When stained with PTA or TI-Blue, nuclei in various tissues, including metastasized cancer cells, were clearly imaged by ASEM without the need for thin-sectioning (Figs. 10 and 12). ASEM observes a 2-3 μm thick specimen layer at 30 kV (Maruyama Y, et al., 2012a; Suga M, et al., 2009; Suga M, et al., 2011), which is comparable to the thickness of the cryo-thin sections used for intraoperative diagnosis. Equipped with a fail-safe system against

film-window breakage (Nishiyama H, et al., 2014), the ASEM has the potential to make diagnoses both quicker and easier, and will be an alternative method for clinical diagnosis. The area of tissues observable by ASEM can be increased by the use of a new multi-windowed ASEM dish, the imaging field of which being 8 times that of the previous single-windowed dish. It will be accelerated even more in the future by increasing the number of windows. Moreover, the open ASEM dish configuration in combination with OM, allows tissue to be manually moved across the flat SiN windows using tweezers (Fig. 13). Two vertical lines of windows, with one vertically displaced to give the region a checkered appearance or a vertically long narrow rectangular window in combination with lateral shift increments realizes efficient monitoring of a large square area, which can be automized by constructing motor-driven auto-manipulator over the dish.

To aid diagnosis by ASEM, nuclei and cytoplasm in the images should be artificially colored blue and red using image recognition algorithms to match their appearance to the standard HE staining-based diagnosis. Immunohistological identification of cancer cells should also be accelerated by using immuno-gold labeling and ASEM, as successfully performed for cells cultured on an ASEM dish (Hirano K, et al., 2014; KinoshitaT, et al., 2014; Maruyama Y, et al., 2012b). Further, cathodoluminescence (CL) could be used to obtain multiple coloring (Nishiyama H, et al., 2014; Thiberge S, et al., 2004).

Today, most kidney biopsies are examined using a combination of three microscopies: OM, immunofluorescence (IF) microscopy and electron microscopy (EM). EM is especially necessary for the diagnosis of the primary glomerulopathies: thin glomerular basement membrane disease, Alport syndrome, fibrillary and/or

immunotactoid glomerulonephritis and minimal change disease (Amann K & Haas CS, 2006). The diagnosis is basically achieved by Epon thin-section TEM (Mochizuki S, et al., 2001), which takes a relatively long time for the embedding and ultra-thin sectioning. By contrast, ASEM of kidney tissue can be completed within 30 min or less using the quick staining method presented here. This, together with the open configuration of the ASEM dish, could accelerate the diagnosis of kidney diseases or be used to obtain a second opinion.

6. Conclusion

In this study, I stained different mouse tissues with UA, TI-Blue, PTA solution or by the NCMIR method, and imaged them in an open aqueous solution at atmospheric pressure by the ASEM. Not only intercellular connections but also cell organelles were clearly observed in tissues at high resolution. Staining with UA was achieved within 15 minutes. After further development of the staining procedure and quick observation of a wider area, the ASEM is expected to be a powerful tool for rapid intraoperative cancer diagnosis and for the diagnosis of kidney diseases. Furthermore, the present study demonstrated that the ASEM can be applied to study the host-microbe interaction that is critical for carcinogenesis in the stomach and also for the body's homeostasis, especially for the acquisition of our natural immunity.

The results presented clearly demonstrate that ASEM is widely applicable not only to basic biology of cells and tissues but also to pathology, including the clinical diagnosis of cancer and the detection of pathogens during surgery and treatment, as well as to food science and industry, including zymology.

Acknowledgments

I thank my major advisor Professor Chikara SATO for his support and guidance. I thank Dr Kazuhiro MIO for his support and guidance. I thank Dr Yuusuke MARUYAMA and Dr Toshio MORIA (AIST) for discussions, during the course of the research. I thank my past and present laboratory fellow Mari SATO and other members for their help and assistance. I thank Dr Tatsuo USHIKI (Niigata University), Dr Shinya SUGIMOTO, Dr Kenichi OKUDA (The Jikei University School of Medicine) and Dr Tom KOUKI (Jichi medical University) for their discussions. I also thank my committee members Professor Haruo NOGAMI, Professor Takashi SHIGA, Professor Ichiro TAKASHIMA and Professor Kenichiro ISHIDA for their suggestions and critical reviews. The work was supported by grants from the Kambayashi Zaydan-in-Aid for Scientific Research and by AIST. I also appreciate Kambayashi Scholarship Foundations Scholarship.

Last but not the least a special thanks to my son Attila and my family members for all the support and patience all these years.

References

ABRAMS IM & MCBAIN JW. (1944). A closed cell for electron microscopy Science **100**, 273-274.

AGRONSKAIA AV, VALENTIJN JA & VAN DRIEL LF. (2008). Integrated fluorescence and transmission electron microscopy. J Struct Biol **164**, 183-189.

AKITA M, TANAKA K & MURAI N. (2013). Detection of CD133 (prominin-1) in a human hepatoblastoma cell line (HuH-6 clone 5). Microsc Res Tech **76**(8), 844-852.

AMANN K & HAAS CS. (2006). What you should know about the work-up of a renal biopsy. Nephrol Dial Transplant **21**(5), 1157-1161.

BAHAR V. (2005). Applications of a novel SEM technique for the analysis of hydrated samples. Microscopy and Analysis **19**(4), 21-23.

BARSHACK I, KOPOLOVIC J, CHOWERS Y, GILEADI O, VAINSHTEIN A, ZIK O & BEHAR V. (2004a). A novel method for "wet" SEM. Ultrastruct Pathol **28**, 29-31.

BARSHACK I, POLAK-CHARCON S, BEHAR V, VAINSHTEIN A, ZIK O, OFEK E, HADANI M, KOPOLOVIC J & NASS D. (2004b). Wet SEM: a novel method for rapid diagnosis of brain tumors. Ultrastruct Pathol **28**(4), 255-260.

BAUERMEISTER DE. (1980). The role and limitations of frozen section and needle aspiration biopsy in breast cancer diagnosis. Cancer **46**, 947-949.

DE JONGE N, PECKYS DB, KREMERS GJ & PISTON DW. (2009). Electron microscopy of whole cells in liquid with nanometer resolution. Proc Natl Acad Sci U S A **106**, 2159-2164.

DEERINCK TJ, BUSHONG EA, THOR A & ELLISMAN MH. (2010). NCMIR methods for 3D EM: a new protocol for preparation of biological specimens for serial blockage scanning electron microscopy. Microscopy, 6-8.

FERREIRO JA, MYERS JL & BOSTWICK DG. (1995). Accuracy of frozen section diagnosis in surgical pathology. Mayo Clinic proceedings **70**, 1137-1141.

GÄHWILER BH, CAPOGNA M, DEBANNE D, MCKINNEY RA & THOMPSON SM. (1997). Organotypic slice cultures: a technique has come of age. Trends Neurosci. **20**(10), 471-477.

GAHWILER BH. (1981). Organotypic monolayer cultures of nervous tissue. J Neurosci Methods **4**(4), 329-342.

GOLGI C. (1898). Intorno alla struttura delle cellule nervose. Bollettino dellaSocietà Medico-Chirurgica di Pavia **13**, 1-14.

HELL SW. (2007). Far-field optical nanoscopy. Science **316**, 1153-1158.

HIRANO K, KINOSHITA T, UEMURA T, MOTOHASHI H, WATANABE Y, EBIHARA T, NISHIYAMA H, SATO M, SUGA M, MARUYAMA Y, TSUJI N, YAMAMOTO M, NISHIHARA S & SATO C. (2014). Electron microscopy of primary cell cultures in solution and correlative optical microscopy using ASEM. Ultramicroscopy **143**, 52-66.

KINOSHITAT, MORI Y, HIRANO K, SUGIMOTO S, OKUDA K, MATSUMOTO S, NAMIKI T, EBIHARA T, KAWATA M, NISHIYAMA H, SATO M, SUGA M, HIGASHIYAMA K, SONOMOTO K, MIZUNOE Y, NISHIHARA S & SATO C. (2014). Immuno-electron microscopy of primary cell cultures from genetically modified animals in liquid

by atmospheric scanning electron microscopy. Microsc Microanal **20**(2), 469-483.

KRISTT D & NYSKA A. (2007). The wet tissue SEM - a new technology with applications in drug development and safety. J Toxicol Pathol **20**(1), 1-11.

KUROKAWA M. (2005). *Color atlas of mouse and an illustrated laboratory manual for brain science Yodosha.*

MARUYAMA Y, EBIHARA T, NISHIYAMA H, KONYUBA Y, SENDA M, NUMAGA-TOMITA T, T., S., M., S. & C, S. (2012a). Direct observation of protein microcrystals in crystallization buffer by atmospheric scanning electron microscopy. Int J Mol Sci **13**(8), 10553-10567.

MARUYAMA Y, EBIHARA T, NISHIYAMA H, SUGA M & SATO C. (2012b). Immuno EM-OM correlative microscopy in solution by atmospheric scanning electron microscopy (ASEM). J Struct Biol **180**(2), 259-270.

MOCHIZUKI S, MORIYA T, NAGANUMA H, NARASAKA T, UENO Y, SATO H, SASANO H & SAITO T. (2001). Significance of fat stains in serial sections from Epon-embedded tissue samples for electron microscopy in renal diseases. Japanese Society of Nephrology **5**, 240–245.

MURAI T, SATO M, NISHIYAMA H, SUGA M & SATO C. (2013). Ultrastructural analysis of nanogold-labeled cell surface microvilli in liquid by atmospheric scanning electron microscopy and their relevance in cell adhesion. International Journal of Molecular Sciences **14**(10), 20809-20819.

NISHIYAMA H, KOIZUMI M, OGAWA K, KITAMURA S, KONYUBA Y, WATANABE Y, OHBAYASHI N, M., F., SUGA M & SATO C. (2014). Atmospheric scanning electron microscope system with an open sample chamber: Configuration and applications. Ultramicroscopy **147C**, 86-97.

NISHIYAMA H, SUGA M, OGURA T, MARUYAMA Y, KOIZUMI M, MIO K, KITAMURA S & C, S. (2010). Atmospheric scanning electron microscope observes cells and tissues in open medium through silicon nitride film. J Struct Biol **172**(2), 191-202.

NISHIYAMA, H., SUGA, M., KOIZUMI, M., OGAWA, K., KONYUUBA, Y., GUARRERA, D. & SATO, C. (2011). Rapid observation with an atmospheric scanning electron microscope. Microscopy and Microanalysis **17**(S2), 510-511.

NYSKA A, CUMMINGS CA, VAINSHTEIN A, NADLER J, EZOV N, GRUNFELD Y, GILEADI O & BEHAR V. (2004). Electron microscopy of wet tissues: a case study in renal pathology. Toxicol Pathol **32**(3), 357-363.

RIEDL O, FITZAL F, MADER N, DUBSKY P, RUDAS M, MITTLBOECK M, GNANT M & JAKESZ R. (2009). Intraoperative frozen section analysis for breast-conserving therapy in 1016 patients with breast cancer. Eur J Surg Oncol **35**(3), 264-270.

RING EA & DE JONGE N. (2010). Microfluidic system for transmission electron microscopy. Microsc Microanal **16**, 622-629.

SAKAI H, FURIHATA M, C., M., TAKAHASHI M, MIYAZAKI H, KONAKAHARA T, IMAMURA T & OKADA T. (2012). Augmented autocrine bone morphogenic protein (BMP) 7 signaling increases the metastatic potential of mouse breast cancer cells. Clin Exp Metastasis **29**(4), 327-338.

SARTORI A, GATZ R, BECK F, RIGORT A, BAUMEISTER W & PLITZKO JM. (2007). Correlative microscopy: bridging the gap between fluorescence light microscopy and cryo-electron tomography. J Struct Biol **160**, 135-145.

SATO C. (2011a). Atmospheric scanning electron microscopy (ASEM) realizes direct EM-OM linkage in solution: aqueous immuno-cytochemistry. JEOL news **46**(1), 17-22.

SATO C. (2011b). Immuno correaltive microscopy in solution using atmospheric scanning electron microscope (ASEM) 大気圧走査電子顕微鏡(ASEM)による水中免疫電顕法. JEOL news **43**, 13-20.

SATO C, MANAKA S, D., N., NISHIYAMA H, SUGA M, NISHIZAKA T, MIYATA M & MARUYAMA Y. (2012). Rapid imaging of mycoplasma in solution using atmospheric scanning electron microscopy (ASEM). Biochem Biophys Res Commun **417**(4), 1213-1218.

SUGA M, NISHIYAMA H, EBIHARA T, OGURA T & SATO C. (2009). Atmospheric electron microscope: limits of observable depth. Microscopy and Microanalysis **15**, 924-925.

SUGA M, NISHIYAMA H, KONYUBA Y, IWAMATSU S, WATANABE Y, YOSHIURA C, UEDA T & SATO C. (2011). The atmospheric scanning electron microscope with open sample space observes dynamic phenomena in liquid or gas. Ultramicroscopy **111**(12), 1650-1658.

TAKAHASHI M, FURIHATA M, AKIMITSU N, WATANABE M, KAUL S, YUMOTO N & OKADA T. (2008). A highly bone marrow metastatic murine breast cancer model established through in vivo selection exhibits enhanced anchorage-independent growth and cell migration mediated by ICAM-1. Clin Exp Metastas **25**(5), 517-529.

TAKAHASHI M, MIYAZAKI H, FURIHATA M, SAKAI H, KONAKAHARA T, WATANABE M & OKADA T. (2009). Chemokine CCL2/MCP-1 negatively regulates metastasis in a highly bone marrow-metastatic mouse breast cancer model. Clin Exp Metastasis. **26**(7), 817-828.

THIBERGE S, NECHUSHTAN A, SPRINZAK D, GILEADI O, BEHAR V, ZIK O, CHOWERS Y, MICHAELI S, SCHLESSINGER J & MOSES E. (2004). Scanning electron microscopy of cells and tissues under fully hydrated conditions. Proc Natl Acad Sci U S A **101**(10), 3346-3351.

WADA N, IMOTO S, HASEBE T, OCHIAI A, EBIHARA S & MORIYAMA N. (2004). Evaluation of intraoperative frozen section diagnosis of sentinel lymph nodes in breast cancer. Jpn J Clin Oncol **34**(3), 113–117.

WILLIAMSON MJ, TROMP RM, VEREECKEN PM, HULL R & ROSS FM. (2003). Dynamic microscopy of nanoscale cluster growth at the solid-liquid interface. Nat Mater **2**, 532-536.

WILSON LB. (1905). A method for the rapid preparation of fresh tissues for the microscope. JAMA **45**(1737).

Figure Legends

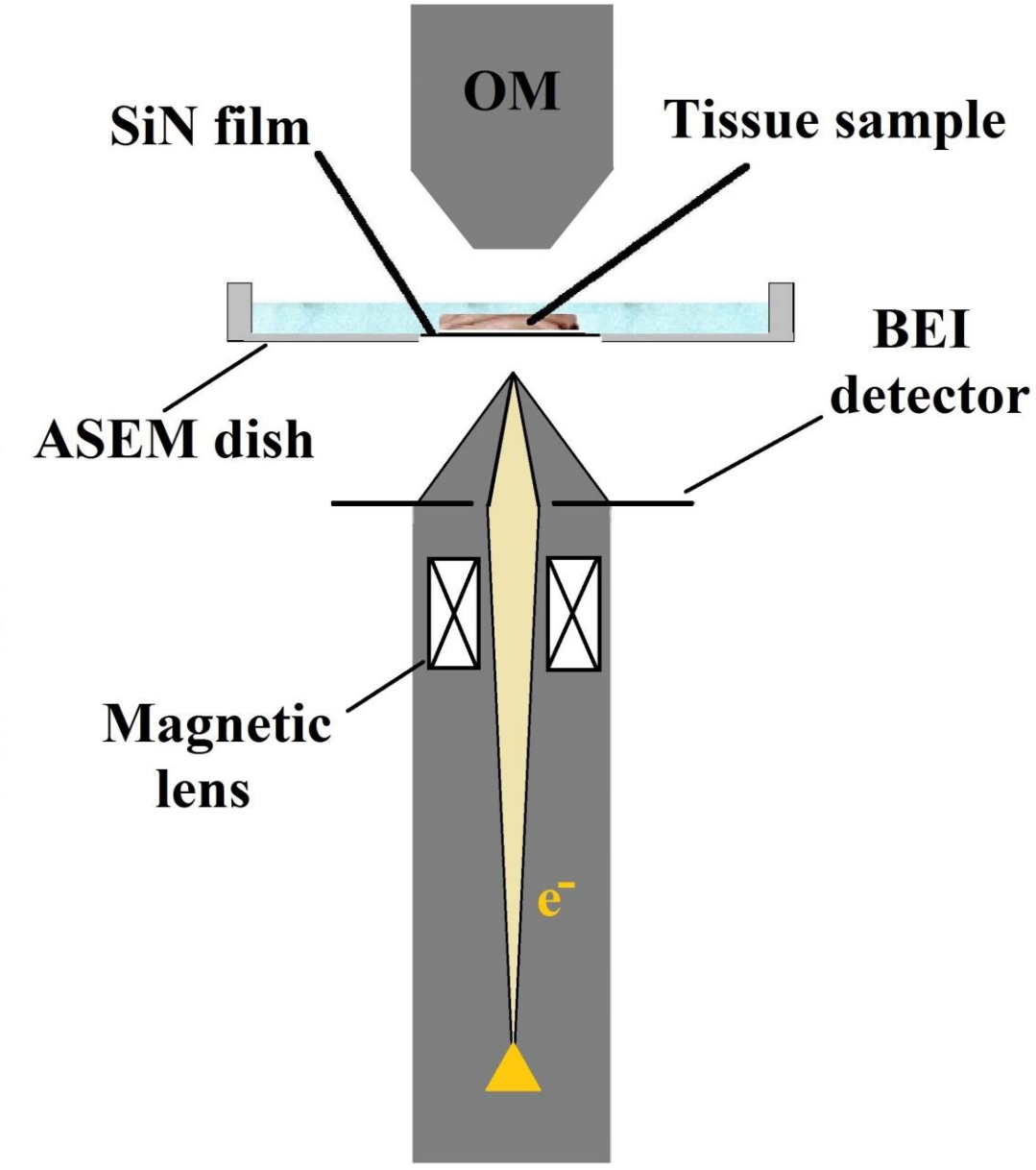

Figure 1. Schematic diagram of the ASEM for tissue observation. In the ASEM correlative microscope, tissue can be observed in aqueous liquid by the SEM from bottom through the SiN film of the ASEM dish and allowing various manipulations from above by OM. Since the optical axes of the two microscopes are aligned, the central region of the sample overview obtained by OM can be imaged immediately afterwards at higher resolution by SEM. Tissues were immersed in radical scavenger D-glucose or ascorbic acid solution and imaged by ASEM.

Figure 2. (A) OM of an HE-stained thin-section, and ASEM images of neural tissues from male mouse, re-fixed with GA, stained with PTA (B-F). In the ASEM images, nuclei are brightly distinguished above the background, while cytoplasm and neurite-like fibers are darker, as they were only weakly stained. (B) A frontal section of the cerebrum showing a layered structure. (C and F) Higher magnification image of the white rectangle in the preceeding panel. Different kinds of neurons with nuclei neurites (arrowheads) are observed. Scale bar 50 μm in A and B panel, 10 μm in C and D, 5 μm in E, 2 μm in F panel.

Sorry!

Currently not opened.

Figure 3. (A) OM of an HE-stained thin-section, and ASEM images of neural tissues from male mouse, re-fixed with GA, stained with PTA (B-F). (B) Horizontal section of the cerebellum. The three clearly different layers, the molecular layer, Purkinji cell layer, the granular layer are visible as well as cerebellar white matter . (C - F) Higher magnification image of the white rectangle in the preceeding panel. Scale bar 50 μm in A and B panel, 20 μm in C, 10 μm in D and E, 2 μm in F panel.

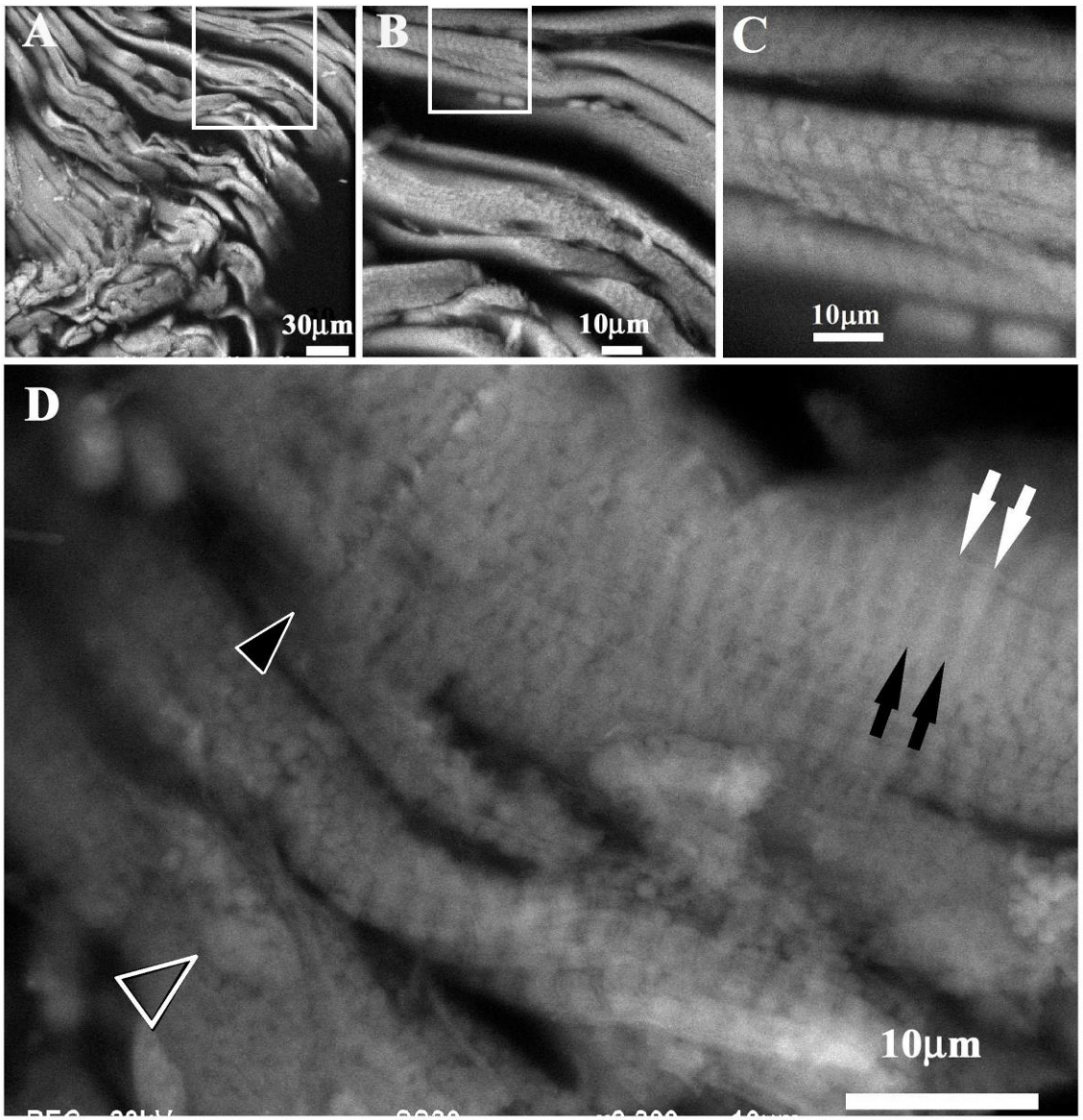

Figure 4. ASEM images of myocardial tissues from male mice (A-C), from female mice (D), re-fixed with GA, stained with PTA.(A) Slab of longitudinal heart tissue observed by ASEM at low magnification. Cardiomyocytes are evident and sometimes branched. (B and C) Higher magnification image of the white rectangle in the preceding panel. Myofibrils can be brightly distinguished above the background. (D) ASEM image of another cardiac muscle area. Nuclei (open white arrowhead) and an intercalated disc (black arrowhead) are visible. Sarcomere striations are visible in myocytes: A-bands (white arrow) are broad bright zones, while I-bands are dark zones (black arrow). Scale bar 30 µm in A, 10 µm in B-D panels.

Figure 5. ASEM images of gastrocnemius muscle from male mice, re-fixed with GA, stained with PTA. (A) Low magnification image. Filaments run along striated muscle fibers. (B) Higher magnification image of the white rectangle in the preceding panel. A white network is evident on the muscle fibers with stripes. (C) The muscle fiber has A-bands, evident as broad bright zones (white downward arrow), and I-bands, evident as dark zones (black upward arrow). Z-lines, look like a faint thin white line in the middle of the I-bands (black arrowhead). Nuclei are bright (white arrowhead). Scale bar 50 μm in A, 10 μm in B and C panels.

Sorry!

Currently not opened.

Figure 6. ASEM images of digestive tract. (A) Low magnification image of the musculus externa of the esophagus from female mice, re-fixed with GA, stained with PTA. (B) Higher magnification image of the white rectangle in the left panel; a longitudinal muscle-like fiber bundle is surrounded by a network. In myocytes, both A- and I-bands are visualized as bright (white arrowheads) and dark zones (black arrowheads), respectively. (C) Low magnification images of the mucosal side of stomach from male mice, re-fixed with GA, stained with PTA. (D) Higher magnification image of the white rectangle in the left panel. Commensalism of bacteria (arrow) is revealed. (E) Mucosal surface of stomach from male mice stained by the modified NCMIR method. (F) Higher magnification of the area indicated by rectangle in E. Symbiotic bacteria (arrow) are brightly observed. (G) Low magnification images of the muscularis externa of the small intestine from male mice, re-fixed with GA, stained with PTA. Longitudinal smooth muscle fibers are aligned in parallel. (H) Higher magnification image of the white rectangle in the left panel. Myocytes containing nuclei (arrowhead) are connected by extracellular filaments, presumably neurons (open arrowhead). Erythrocytes (arrow) are also visible. Scale bar: 20 μm in A and G; 10 μm in B, C, E and H; 5 μm in D and F.

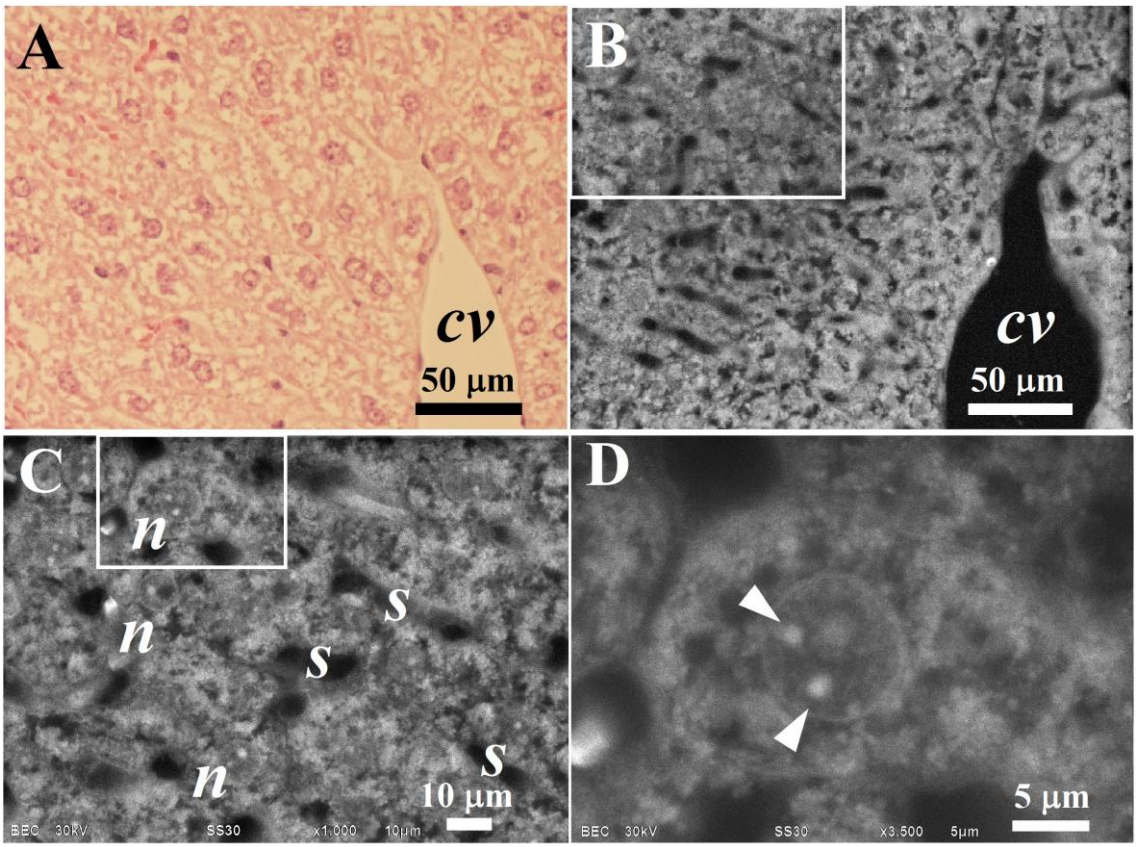

Figure 7. ASEM images of liver from male mice, re-fixed with GA, stained with PTA. (B-D). (A) OM images of an HE-stained thin-section. (B) Low magnification image of a tissue slab stained with PTA. Hepatic cords, sinusoids and central vein (*cv*) are visible. (C and D) Higher magnification image of the white rectangle in the preceeding panel. Hepatocytes with their nucleus (*n*) and nucleoli (arrowhead), sinusoids (*s*) are shown. Scale bar: 50 µm in A and B, 10 µm in C, 5 µm in D panel.

Sorry!

Currently not opened.

Figure 8. (A) OM images of paraffin section of kidney stained with HE. ASEM image of kidney cortex from female mice, re-fixed with GA, stained with PTA (B). The features evident in the characteristic view are putatively assigned as indicated: Bowman's capsule (BC), podocytes (visceral epithelial cells; arrowheads), a glomerulus (G), proximal convoluted tubules (PCT), distal convoluted tubules (DCT). Scale bar: 50 μm.

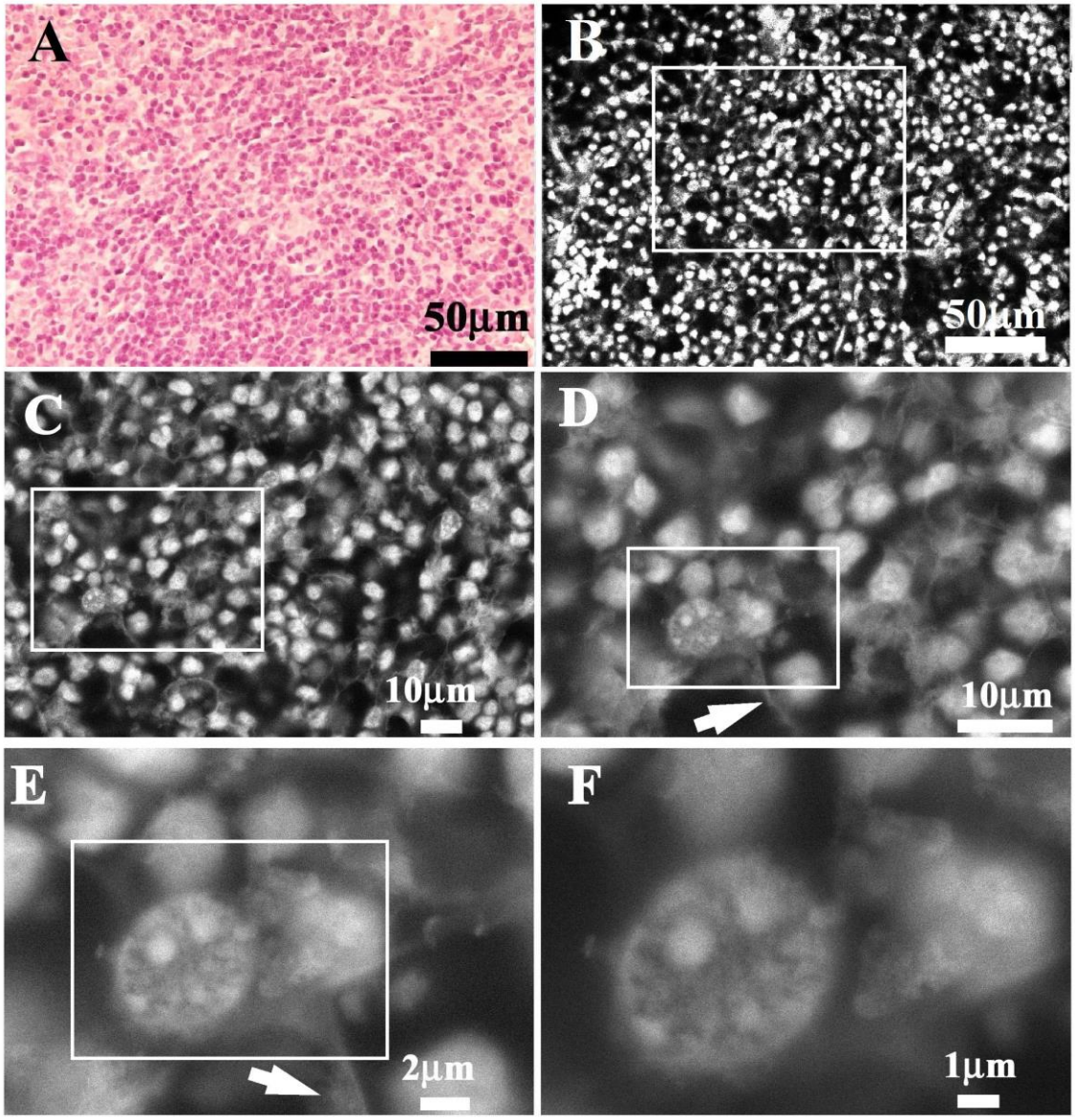

Figure 9. OM images of paraffin section of spleen stained with HE (A) and ASEM images of spleen stained from female mice, re-fixed with GA, stained with PTA (B-F). (A) OM images of the white pulp of spleen. (B) The spleen was cut to obtain 200 μm-thick tissue slabs, stained with PTA and observed at low magnification by ASEM. (C-F) Higher magnification ASEM images of the white rectangle in the preceding panel. Differently shaped blood cells, presumably including lymphocytes, were observed. Reticular fiber-like fibrous structures (arrow) less than 2 μm in thickness, were also observed. Scale bar: 50 μm in A and B; 10 μm in C and D; 2 μm in E; 1 μm in F panel.

Sorry!

Currently not opened.

Figure 10. Comparative OM (A and E) or ASEM (B-D and F-H) observation of control lung (A-D) and lung metastasized by breast cancer cells (E-H). (A) OM of an HE-stained thin-section of control lung. (B) Low magnification ASEM image of control tissue slab stained with both TI-Blue and PTA. Alveoli with alveolar ducts are visible. (C-D) Higher magnification images of the white rectangle in the upper panel. Nuclei of normal size are observed (arrowhead). (E, F, G and H) Comparative observation of tissue excised from a lung metastasized with breast cancer cells. (E) OM of an HE-stained thin-section. (F-H) ASEM of TI-Blue- and PTA-stained thick slab at the same magnification as the corresponding left panels. Regular alveoli, alveolar ducts and alveolar cells are only faintly discernable. Most of the space is occupied by cells of different shapes with larger nuclei (arrow), i.e., cancer cells. Scale bar: 50 μm in A, B, E, F; 10 μm in C, D, G, H.

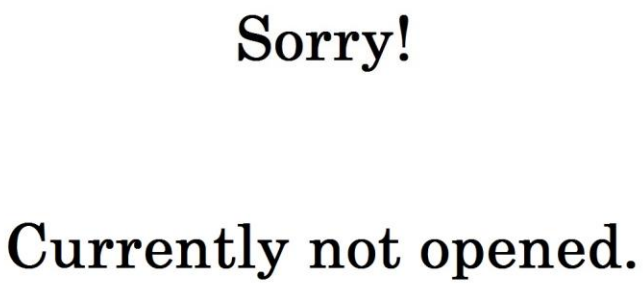

Figure 11. Comparative ASEM observation of spinal cord metastasized by breast cancer cells and its control. (A-B) ASEM image of a control spinal cord tissue slab stained with both TI-Blue and PTA. One of nuclei is shown along the spinal cord (arrowhead). (C-D) Comparative observation of tissue excised from a spinal cord metastasized with breast cancer cells. A cluster of unusually large nuclei similar to those seen in lung metastasized by breast cancer cells (Fig. 10F-H) were observed (arrowhead). Scale bar: 50 μm in A and C; 10 μm in B and D.

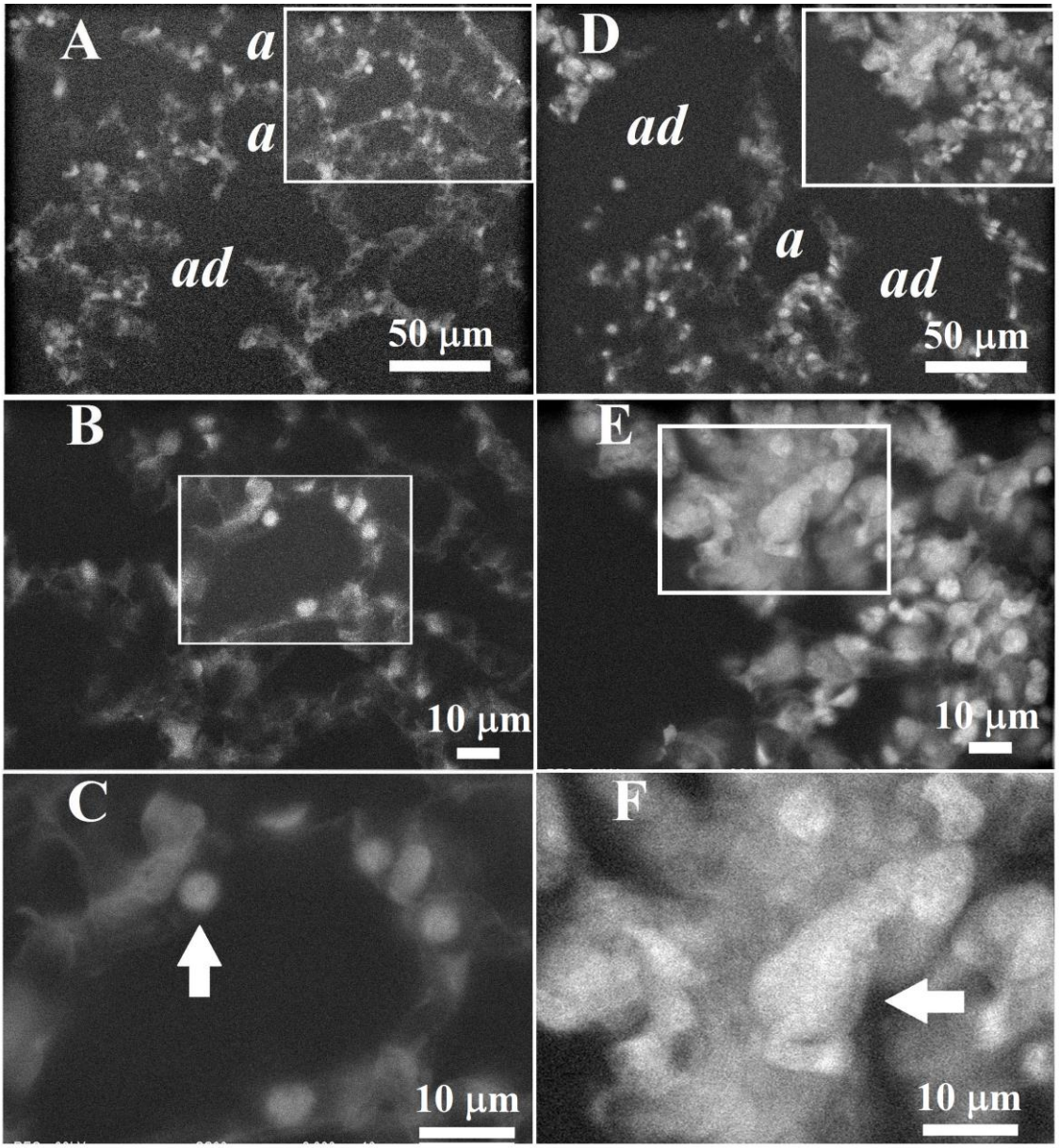

Figure 12. Quick observation of the normal lung (A-C) and the lung metastasized by breast cancer cells (D-F). Lung tissue slabs without perforation were quickly stained with UA for 15 minutes and observed by ASEM. (A-C) ASEM images of tissue slab of a normal lung. A normal thin wall structure with alveoli (*a*) and alveolar ducts (*ad*) was observed. The cell nuclei (arrow) located at the surface of the slab were brightly imaged. (D-F) Tissue excised from a lung metastasized by breast cancer cells. Lung structures look fainter in the metastasized area (top right). Instead, the structure was occupied by the cells with unusually large nuclei (arrow), similar to those stained with PTA/TI-Blue (Fig. 10F-H). Scale bar: 50 μm in A, D; 10 μm in B, E, C, F.

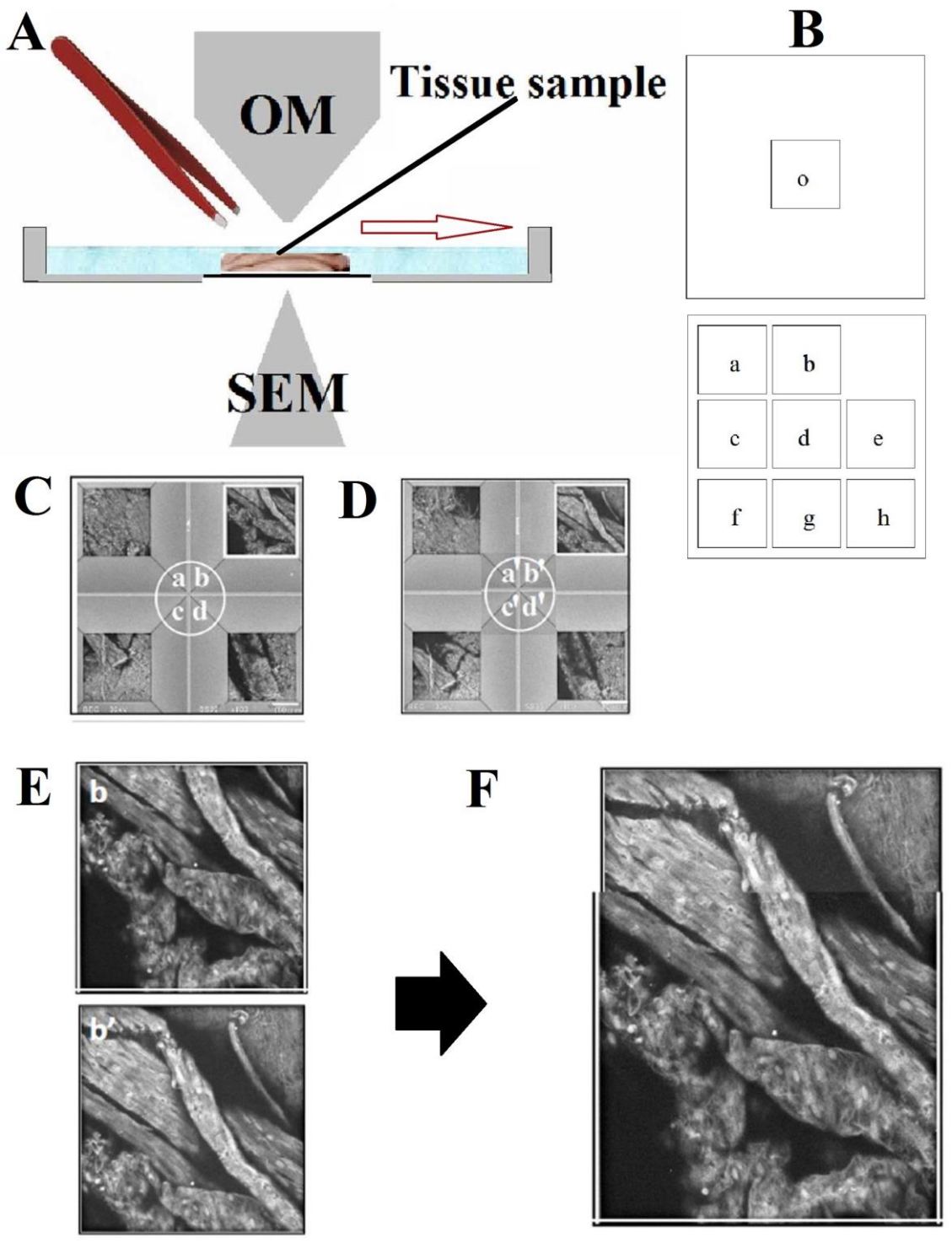

Figure 13. Wide area imaging by shifting a tissue on the ASEM dish. (A) Schematic diagram of the procedure. The shift caused by pushing with the tweezers is precisely controlled by low magnification monitoring using the upper OM (see Fig. 1A). (B) Schematic diagrams of a one-window and an 8-window ASEM dish. All windows are 250 x 250 μm. (C) Spinal cord images initially recorded from windows a, b, c, d. (D)

Images recorded in the same windows after the tissue has been pushed in one direction causing it to slip across the SiN-film window. (E) Higher magnification image of window b in panel C and of window b’ in panel D. (F) Merged image of windows b and b’ shown in (E).